Real-time inversion of VLP source functions at Stromboli Volcano, Italy.

Emmanuel Auger (1), Luca D'Auria (1), Marcello Martini (1),
Bernard Chouet (2), Phillip Dawson (2)
(1) Istituto Nazionale di Geofisica e Vulcanologia - Osservatorio Vesuviano
(2) United States Geological Surveys - Menlo Park

March 15, 2006

Abstract

We present a comprehensive processing tool for the real-time analysis of the source mechanism of Very-Long-Period (VLP) seismic data based on waveform inversions performed in the frequency domain for a point source. A search for the source providing the best-fitting solution is conducted over a three-dimensional grid of assumed source locations, in which the Green's functions associated with each point source are calculated by finite differences using the reciprocal relation between source and receiver. Tests performed on 62 nodes of a Linux cluster indicate that the waveform inversion and search for the best-fitting signal over 100,000 point sources require roughly 30 s of processing time for a 2-min-long record. The procedure is applied to post-processing of a data archive and to continuous automatic inversion of real-time data at Stromboli, providing insights into different modes of degassing at this volcano.

1 Introduction

Very-Long-Period (VLP) seismic events commonly accompany magmatic and/or hydrothermal transport [4] [3]. The determination of the source location and source mechanism gives important informations about geometries of volcanic conduits and their volumetric variations during pre- and sin-eruptive phenomena [13] [16] [8] [10] [2] [9]. For this reason we developed applied VLP source function inversion for the monitoring of Stromboli volcano.

This paper demonstrates the feasibility of obtaining real-time estimates of the source location and source mechanism of VLPs at Stromboli from continuous, automatic inversion of VLP waveforms recorded by a dense broadband network using a new powerful inversion scheme in the frequency domain. In our procedure, inversions are carried out over many point sources, thus removing the preliminary requirement for knowledge of an initial trial source position. We demonstrate the usefulness of this approach for processing both real-time data and large data archives.

2 Stromboli Volcano

Stromboli is the northernmost active volcano of the Aeolian island arc in the Tyrrhenian sea (Fig. 1). Following a landslide and tsunami on 30 December 2002, and subplinian eruption on 5 April 2003, Stromboli has become the focus of particular attention from the scientific community and Italian Civil Protection. Since January 2003, INGV (Osservatorio Vesuviano) has maintained a 13-station network of broadband seismometers on this volcano (Fig. 1). Real-time data transmission allows continuous remote monitoring of Strombolian activity, which is normally characterized by mild, intermittent explosive activity [7]. VLP waveforms radiated by these explosions have been analyzed by [6], who determined that their source mechanisms include both moment-tensor and single-force components. The study of [6] is representative of activity recorded over an interval of a single week in September 1997, and thus provides only a momentary glimpse of Strombolian activity. As a result of current monitoring, a large archive of VLP events is now available for Stromboli. Such archive provides a unique opportunity for further analyses of the source mechanisms of Strombolian activity and better understanding of long-term temporal trends in Strombolian dynamics.

3 Frequency-domain inversion for moment tensor and single force

The displacement field generated by a point seismic source, can be expressed as [4] [16] [6] [5]:

$$u_n(t) = \sum_{i=1}^{N_m} m_i(t) * G_{ni}(t), \tag{1}$$

where $u_n(t)$ is the n-component of seismic displacement at a receiver at time t, $m_i(t)$ is the time history of the i-th moment-tensor or single-force component at the source, $G_{ni}(t)$ are the Green's functions corresponding to each of the respective moment-tensor and single-force components, and N_m is the number of source mechanism components.

Once Green's functions are known, the nine $m_i(t)$ in eq. (1) are retrieved through least squares inversion expressing the standard linear problem $d = Gm$ in eq. (1). The classic approach ([17] [16] [6] [5]) considers the convolution relation 1 in the time domain:

$$u_n(t) = \sum_{i=1}^{N_m} \int_{-\infty}^{+\infty} m_i(\tau) \cdot G_{ni}(t-\tau) d\tau. \tag{2}$$

Discretization of the integral over time in this equation usually leads to a very large square matrices whose dimension represents the product of the number of generalized moment components, N_m, times the number of time increments, N_τ, used in the convolution operation. As each element of this matrix is itself obtained through a time consuming convolution, the computing of the matrix lasts more than the matrix inversion.

Our strategy to speed up the inversion scheme relies on performing the inversion in the frequency domain. This approach is similar to deconvolution operations commonly carried out in seismic exploration, where large datasets are common [18]. The Fourier transform of eq. 2 is given by:

$$u_n(\omega) = \sum_{i=1}^{N_m} m_i(\omega) \cdot G_{ni}(\omega). \tag{3}$$

In this expression, for each frequency, we only need to invert a small matrix with dimension N_m times the number of receiver channels. This approach, involving repeated inversion of many small matrices is computationally more efficient than that requiring the inversion of a single large matrix. Tests carried out with the discretized model of Stromboli described below, indicate that this scheme is some 200 times faster than that used by [6]. Fig.2 compares our results with those obtained by [6] for an explosion recorded in September 1997 and displayed in Fig.11 in [6]. Apart from slight discrepancies in the very-low frequency component of the vertical component of force F_z, the results obtained by the two approaches are found to match each other precisely. For this comparison, an 18-s-long record (901 samples, 451 frequencies) centered on the event was considered.

The computation of Green's functions, by a 3D elastic finite difference method ([15]) is not a simple task. In our case we computed G.f.s over a huge grid with 100,000 grid nodes spaced 40 m, for a total source volume of 6.4 km^3 (Fig. 1). A dramatic reduction in computation times is achieved using the reciprocity theorem [1]:

$$G_{ni}(r, s) = G_{in}(s, r). \tag{4}$$

Here, the Green function $G_{ni}(r, s)$ expresses the n-component of displacement at r due to a unit impulse applied in the i-direction at s. Using reciprocity, the three components of displacement can be calculated at each source node for impulsive forces applied in the x, y and z directions at each receiver in the network. The Green's functions for moment components in eq.3 are then easily derived from the Green's functions associated with the forces through spatial derivations of $G_{ni}(r, s)$ with respect to the source coordinates s. In this way, the total number of required computations is limited to just three times the number of receivers.

4 Applications : Real-time inversion and massive processing of archive data

Our first application of the frequency-domain inversion focuses on the processing of waveform data archived since January 2003. To demonstrate the feasibility of processing long periods of time we processed the time interval 10-19 September 2004. This represents a period of enhanced Strombolian activity during which strong explosions were occurring. During that time span, 2001 events were detected by the automatic semblance processing system EOLO [11] [12]. The event locations obtained from waveform inversion are densely clustered at an elevation of $\sim$ 500 m in the northwest quadrant of the volcano, roughly 300 m

to the southeast of the semblance maximum detected by EOLO (Fig. 3). The clustered locations coincide with the position of source of Type-1 event studied by [6], 220 m beneath and $\sim$ 160 m northwest of the active vents. In this data set 540 events (27% of the total) are located exactly on the same position as the Type-1 event in Chouet's study, 600 events (30% of the total) are found within 80 m (2 grid nodes) of that position, and the remaining events scatter along a trend in the WNW-ESE direction.

The statistical distribution of event locations suggests that a single source was active during this time interval and yields no evidence for a second, distinct source. The source locations obtained from waveform inversion display significantly less scatter compared to the locations obtained from semblance analysis. Location errors can be estimated from the widths of the statistical distributions (Fig.4). This yields errors of roughly 150, 50, and 60 m in the x (east), y (north), and z (vertical) directions, respectively.

We computed the uncertainty on the event location using probabilistic estimation [14]. From the misfit function, between computed and synthetic waveforms, a posterior probability density function is obtained. Using this function we can compute a confidence ellipse. Fig.3 shows the major axis of the 68% confidence ellipsoid for two representative events, one of which is co-located with the Type-1 source analyzed by [6], and the other is representative of events belonging to the WNW-ESE-trending distribution of scattered source locations. The uncertainty for the event co-located with the Type-1 source is about four times smaller than that associated with the event representative of the scattered sources.

The VLP seismicity at Stromboli sampled during a week in September 2004 shows a high repeatability among some events (Fig.5, see events in Class 1). Such events share the same waveform characteristics as the Type-1 event analyzed by [6]. A few other well-resolved events show the characteristics of Type-2 events analyzed by [6], while other events show durations and frequency contents that are distinct from the two event types observed by [6] (*e.g.*, the event in Class 2 in Fig.5). Such results point to the existence of modes of degassing that are distinct from those already imaged by [6].

For our next application, we consider the real-time inversion of data. Our procedure involves two steps, namely, (1) detection of an event in the data stream, and (2) inversion of the detected event to obtain its location and source-time history. In the first step, an inversion is carried out over a 2-min-long window, with 1 min overlap. To detect the presence of a VLP event inside the window we compute the 68% confidence ellipsoid as described above. When a VLP event is present in the window, the ellipsoid is small and centered at or near the VLP source. In the second step, following the detection of an event a new window is cut into the data stream in such a way that the center of the window is aligned with the peak ground displacement recorded at a reference station. An inversion is then performed on this centered window. Fig. 6 shows the result of applying this procedure to data in a 1-hour-long window.

We note in Fig. 6 that every occurrence of a VLP event has been successfully detected by our automatic inversion. The source-time functions of moment in Fig. 6 display a wide range of magnitudes and shapes. Examples of this variety of behavior are the sharp pulse of moment observed at 12:53:30, and the low-frequency, low-amplitude event at 12:37:20.

5 Conclusions

We have shown how, performing waveform inversion in the frequency domain and using reciprocity, a dramatic drop in computation times is achieved. This allows both for reprocessing of large datasets and for real-time analysis.

We first analyzed 2001 events that occurred during 10 days in September 2004. In this time span, waveforms, showed a high degree of similarity, but with some significant outlier. Processing of the three-year-long archive gathered at Stromboli should advance our knowledge of its dynamics.

In a second step, we demonstrated the feasibility of performing continuous, real-time inversions of the data from the Stromboli network. Analyses performed over a 1-hour-long window indicate that our inversion scheme is capable of detecting a wide range of VLP events and quantifying their source processes. Following [4], we are currently developing a procedure to automatically analyze the moment tensor and retrieve the geometry of the portion of conduit where the VLP event originates. This approach holds the promise that sudden increases in the volume of gas ejected, or other radical changes in the magma feeding system might be detected and quantified as they occur, thereby affording a robust real-time monitoring tool.

References

[1] Aki, K., and P. G. Richards, *Quantitative Seismology: Theory and methods.* 932 pp., W. H. Freeman, New York, 1980.

[2] Almendros, J., and B. Chouet, Performance of the radial semblance method for the location of very long period volcanic signals. Bull. Seism. Soc. Amer. 93(5), 1890–1903, 2003.

[3] Aster, R., J. Lees, and J. Neuberg, Broadband seismic and acoustic observations of volcanic seismicity. 2000.

[4] Chouet, B., New methods and future trends in seismological volcano monitoring. In Scarpa and Tilling, editors, *Monitoring and Mitigation of Volcano Hazards*, pages 23–97, Springer-Verlag, New York, 1996.

[5] Chouet, B., P. Dawson, and A. Arciniega-Ceballos, Source mechanism of Vulcanian degassing at Popocatpetl Volcano, Mexico, determined from waveform inversions of very long period signals. J. Geoph. Res. 110, B07301, doi:10.1029/2004JB003524, 2005.

[6] Chouet, B., P. Dawson, T. Ohminato, M. Martini, G. Saccorotti, F. Giudicepietro, G. De Luca, G. Milana, and R. Scarpa, Source mechanisms of explosions at Stromboli Volcano, Italy, determined from moment-tensor inversions of very-long-period data. J. Geoph. Res. 108(B1), 2019, doi:10.1029/2002JB001919, 2003.

[7] Chouet, B., N. Hamisevicz, and T. R. McGetchin, Photoballistics of volcanic jet activity at Stromboli, Italy. J. Geoph. Res. 79, 4961–4976, 1974.

[8] Chouet, B., G. Saccorotti, P. Dawson, M. Martini, R. Scarpa, G. De Luca, G. Milana, and M. Cattaneo, Broadband measurements of the sources of

explosions at Stromboli Volcano, Italy. Geoph. Res. Lett., 26(13), 1937–1940, 1999.

[9] Dawson, P., D. Whilldin, and B. Chouet, Application of near real-time radial semblance to locate the shallow magmatic conduit at Kilauea Volcano, Hawaii. Geoph. Res. Lett., 31, L21606, doi:10.1029/2004GL021163, 2004.

[10] Kawakatsu, H., S. Kaneshima, H. Matsubayashi, T. Ohminato, Y. Sudo, T. Tsutui, K. Uhira, H. Yamasato, H. Ito, and D. Legrand, Aso94: Aso seismic observation with broadband instruments. J. Volc. Geoth. Res. 101, 129–154, 2000.

[11] D'Auria, L., - The automatic monitoring system of Stromboli, http://eolo.ov.ingv.it.

[12] D'Auria, L., M. Martini, E. Auger, F. Giudicepietro, W. De Cesare, and G. Scarpato, Real-time automatic seismic monitoring of Stromboli using massive parallel computing, In *IAVCEI General Assembly, Pucn, Chile*, November 2004.

[13] Matsubayashi, H., The source of the long period tremors and the very-long period events preceding the mud eruption at Aso Volcano, Japan. (in Japanese with English abstract), M. A. thesis, Tokyo Univ., Tokyo, 1995.

[14] Mosegaard, K., and A. Tarantola, Probabilistic Approach to Inverse Problems. In Lee, Kanamori, Jennings, and Kisslinger, editors, *International Handbook of Earthquake and Engineering Seismology*, pages 237–265, Academic Press, New York, 2002.

[15] Ohminato, T., and B. A. Chouet, A free-surface boundary condition for including 3D topography in the finite-difference method. Bull. Seism. Soc. Amer. 87(2), 494–515, 1997.

[16] Ohminato, T., B. A. Chouet, P. Dawson, and S. Kedar, Waveform inversion of very long period impulsive signals associated with magmatic injection beneath Kilauea Volcano, Hawaii. J. Geoph. Res.103(B10), 23,869–23,862, 1998.

[17] Uhira, K., and M. Takeo, The source of explosive eruptions of Sakurajima Volcano, Japan. J. Geoph. Res. 99(B9), 17,775–17,789, 1994.

[18] Yilmaz, O., *Seismic Data Processing*, Society of Exploration Geophysicists, 1987.

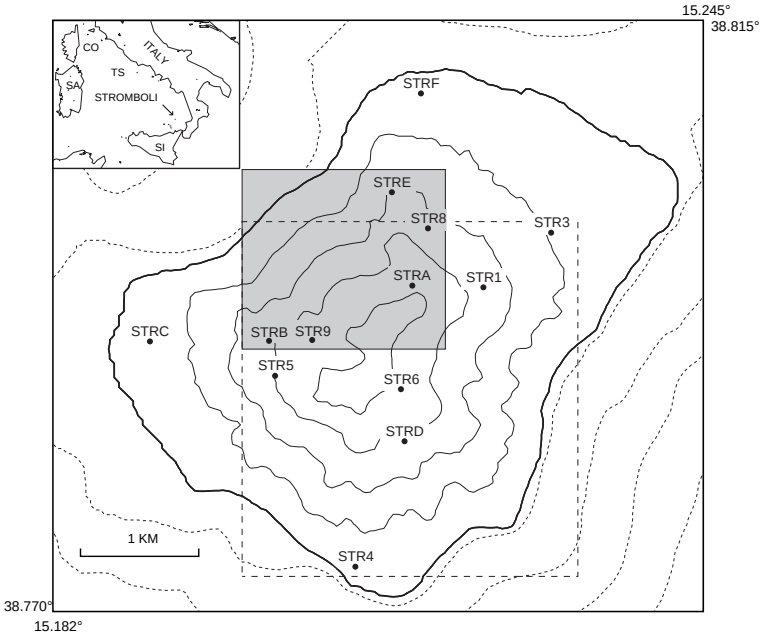

FIGURE 1

Figure 1: Map of Stromboli Volcano showing locations of three-component broadband stations (solid dots) on Stromboli Volcano. The square bounded by the dashed perimeter bounds the horizontal extent of the volume within which a search for the point source providing the best-fitting waveforms is carried out. The vertical extent of this volume ranges from 460 m below sea level to 740 m above sea level. The gray-shaded rectangle marks the horizontal extent of the source region illustrated in Figure 3 (see text for details). Contour lines represent 200 m contour intervals. The inset shows the location of Stromboli in the Tyrrhenian Sea.

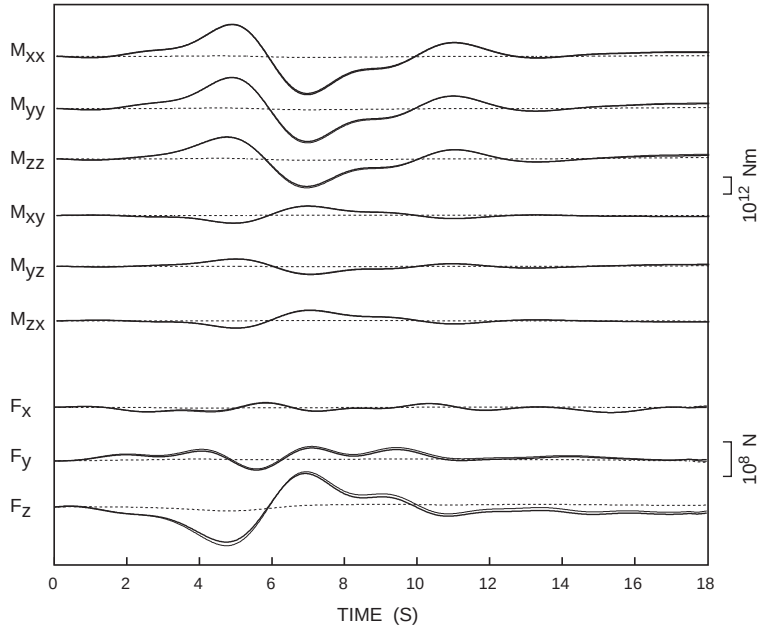

FIGURE 2

Figure 2: Comparison between the generalized moment-tensor solution obtained by [6] (thin line) and generalized moment tensor obtained in the present study (bold line). Dotted lines represent the difference between the two solutions. The two solutions coincide most of the time, showing only a slight discrepancy in the lowest frequency component of the vertical force.

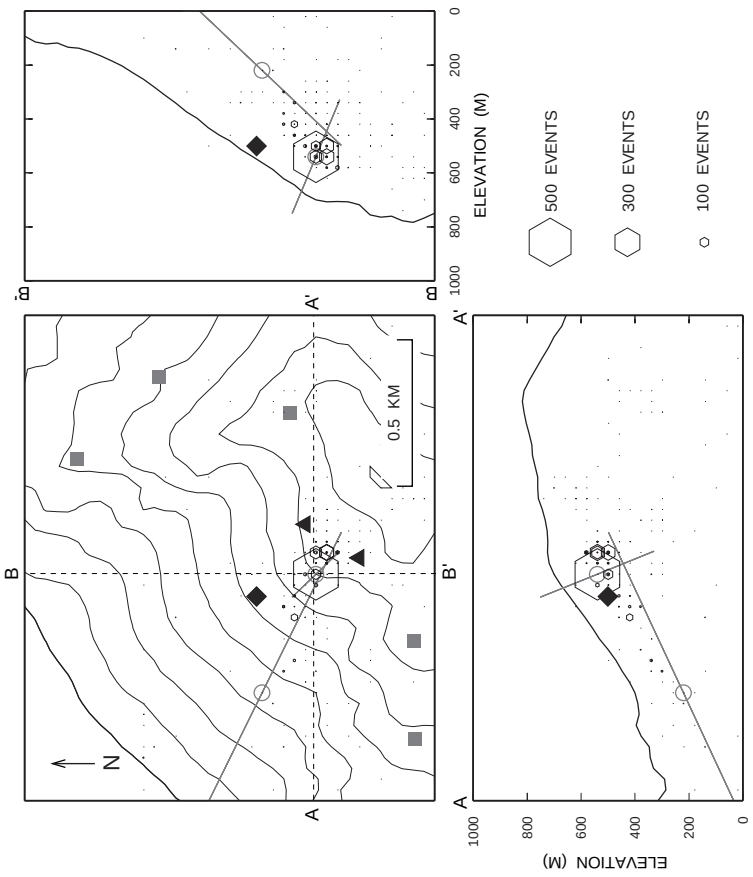

FIGURE 3

Figure 3: Detail of the northwest quadrant of Stromboli (gray-shaded rectangle in Figure 1) showing the locations of events that occurred during the interval September 10-19, 2004. Of the total of 2001 events, 1886 (94%) are located within this zone. The upper left panel is a map view, in which gray squares mark receivers and black triangles mark the active vents in the crater of Stromboli. Contour lines represent 100 m contour intervals. In the upper right and bottom panels the topography is plotted along two vertical cross sections, whose positions are indicated by the dashed lines (A-A' and B-B') in the map view. In each panel, hexagons mark the locations of VLP events projected unto the cross sectional plane, with size of the hexagons proportional to the number of events per grid node. The black diamond marks the mean position of these events obtained by semblance. The location of the largest hexagon, where 27% of the total of 2001 events cluster, coincides with the location of the source of the Type-1 event analyzed by [6]. Two events, whose locations are indicated by light gray circles, are shown together with a thick gray line marking the major axis of the 68% confidence ellipsoid (see text for explanations).

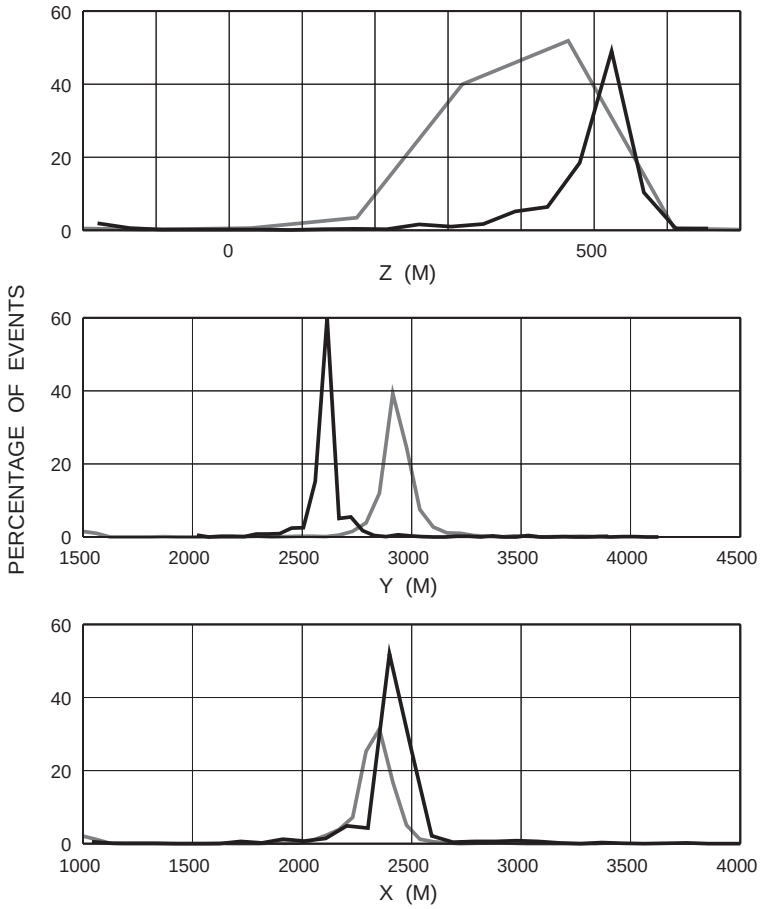

FIGURE 4

Figure 4: Comparison between locations obtained by semblance analysis (gray line) and locations obtained by waveform inversions (black line). The data set includes 2001 events that occurred during the interval September 10-19, 2004.

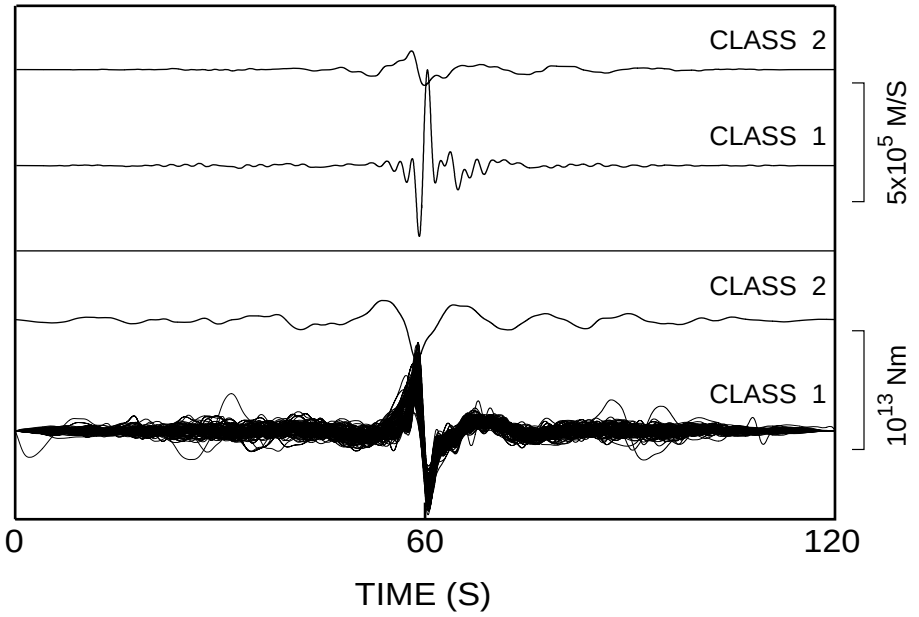

FIGURE 5

Figure 5: Selection of 127 events among the 540 that are located at the same position as the Type-1 event analyzed by [6]. 126 events with semblance higher than 0.97 are grouped in Class 1. Class 2 contains a single event. The top panel shows the EW component of ground velocity at station STRA (see Figure 1) for a representative event in each class, and the bottom panel shows the moment component M_{zz} for all events in the two classes.

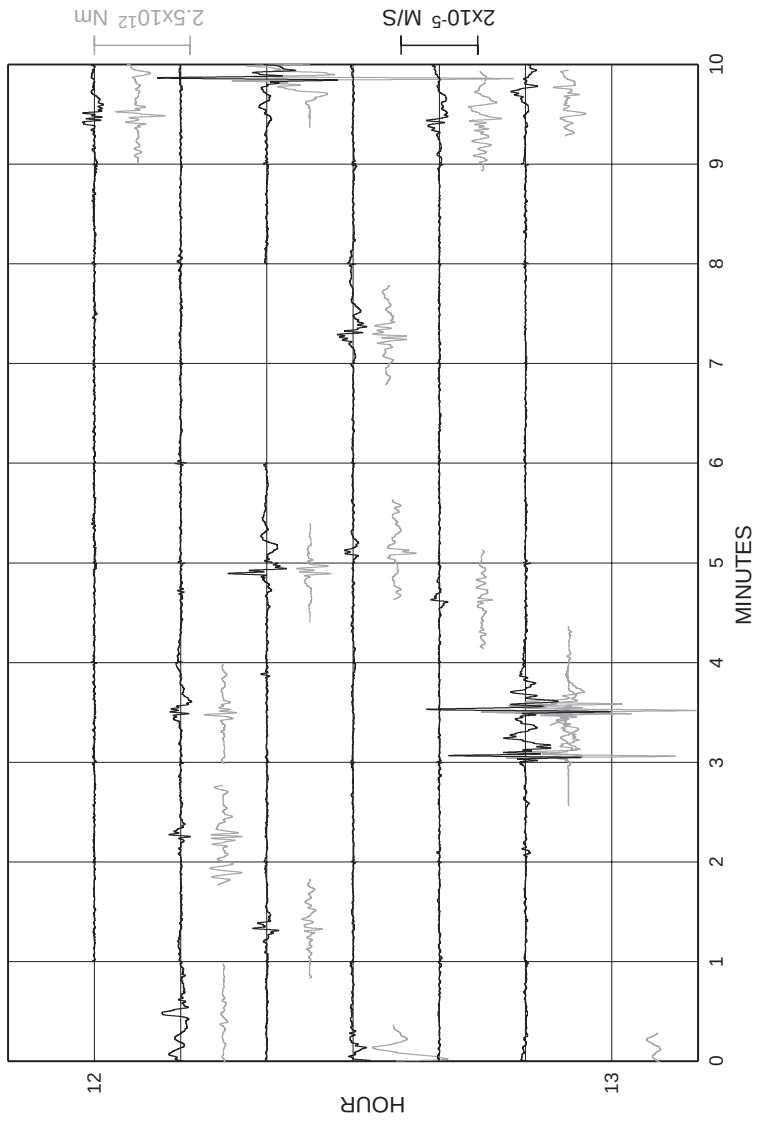

FIGURE 6

Figure 6: Results of continuous, real-time inversion for the 12-13-hour interval on 30 September 2004. The black line represents the EW component of ground velocity recorded at station STRA (see Figure 1), and the gray line represents the time history of the moment trace $M_{xx} + M_{yy} + M_{zz}$ for the detected VLP events (see text for details). For each inversion window, the plot shows only the central 1-min section of the solution, which coincides with the untapered part of the seismograms. To help visualize the results, the trace of the moment is vertically offset from the velocity trace. The gray scale is the moment scale and the black scale is the ground velocity scale.